

SUPPLEMENTARY INFORMATION

**The impact of the length of alkyl chain on the behavior of  
benzyl alcohol homologous - the interplay between  
dispersive and hydrogen bond interactions**

N. Soszka<sup>1,2</sup>, B. Hachuła<sup>1,2\*</sup>, M. Tarnacka<sup>2,3</sup>, E. Kamińska<sup>4</sup>, J. Grelska<sup>2,3</sup>,  
K. Jurkiewicz<sup>2,3</sup>, M. Geppert-Rybczyńska<sup>1</sup>, R. Wrzalik<sup>2,3</sup>, K. Grzybowska<sup>2,3</sup>,  
S. Pawlus<sup>2,3</sup>, M. Paluch<sup>2,3</sup>, K. Kaminski<sup>2,3</sup>

<sup>1</sup> *Institute of Chemistry, University of Silesia in Katowice, Szkolna 9, 40-006 Katowice, Poland*

<sup>2</sup> *Silesian Center for Education and Interdisciplinary Research, 75 Pulku Piechoty 1a, 41-500 Chorzow, Poland*

<sup>3</sup> *August Czerwinski Institute of Physics, University of Silesia in Katowice, 75 Pulku Piechoty 1, 41-500 Chorzow, Poland*

<sup>4</sup> *Department of Pharmacognosy and Phytochemistry, Faculty of Pharmaceutical Sciences in Sosnowiec, Medical University of Silesia in Katowice, Jagiellońska 4, 41-200 Sosnowiec, Poland*

\*Corresponding author: (B.H.) barbara.hachula@us.edu.pl

## Results of Density and Refractive index measurements

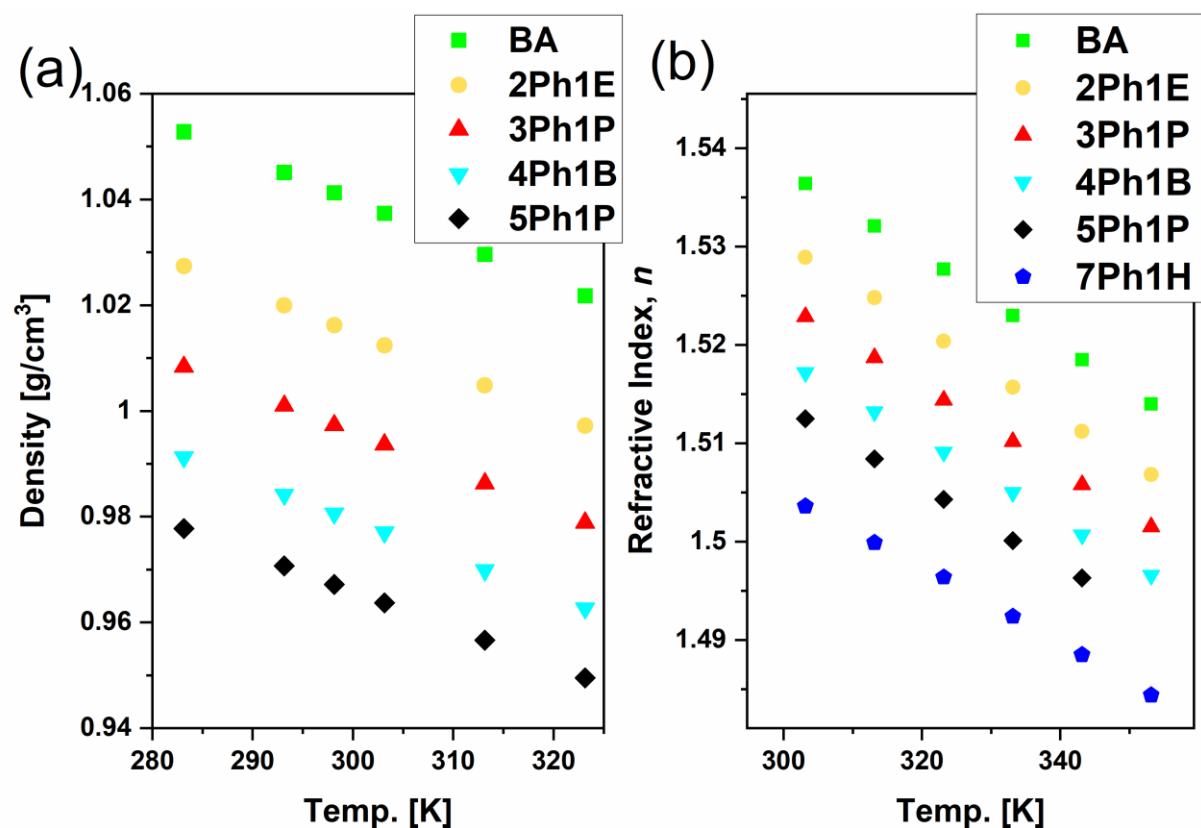


**Figure S1.** Density (a) and refractive index (b) of PhAs at different temperatures.

## Results of Fourier transform infrared (FTIR) spectroscopy

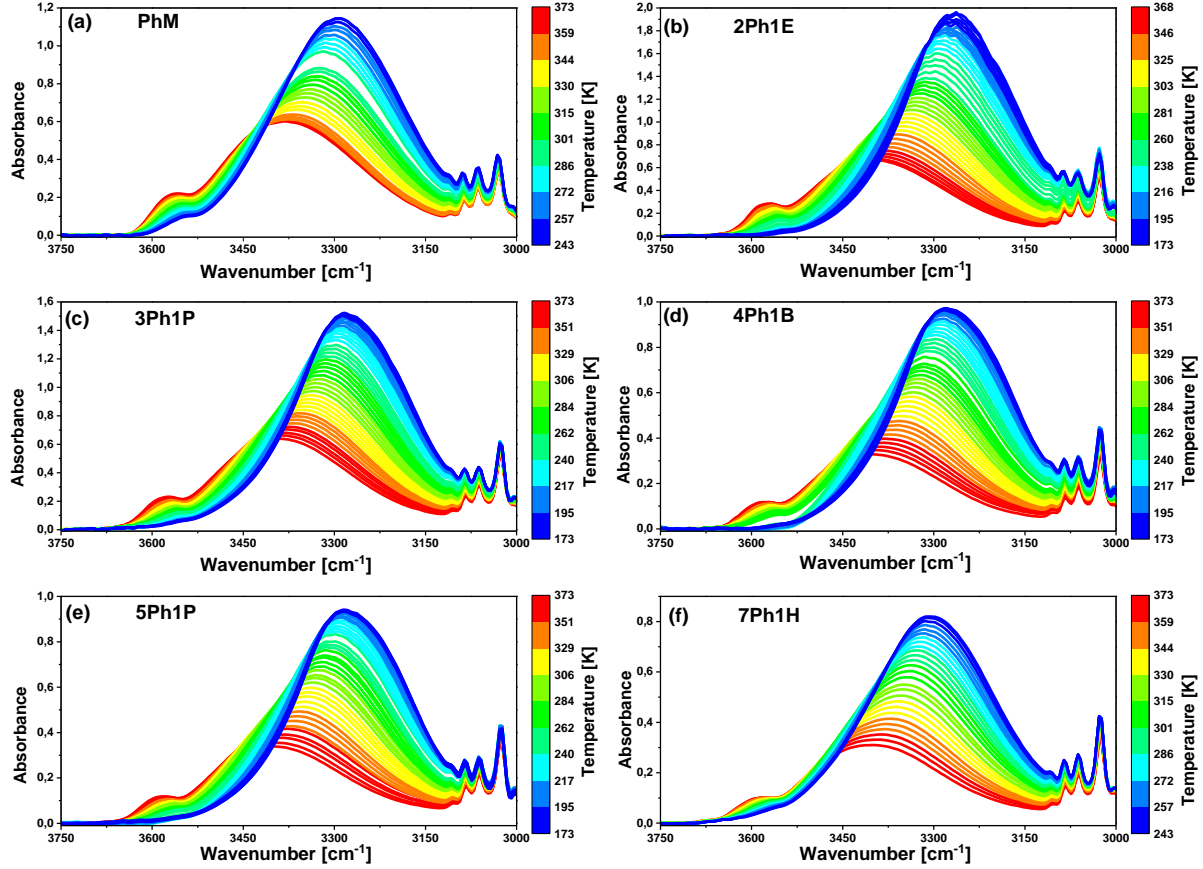


**Figure S2.** Temperature-dependent FTIR spectra in the range 3800 – 3000 cm<sup>-1</sup> measured from 173 K to 373 K for PhAs (b-e), except for PhM and 7Ph1H (a, f) for which the spectra were collected in the temperature range 243 – 373 K.

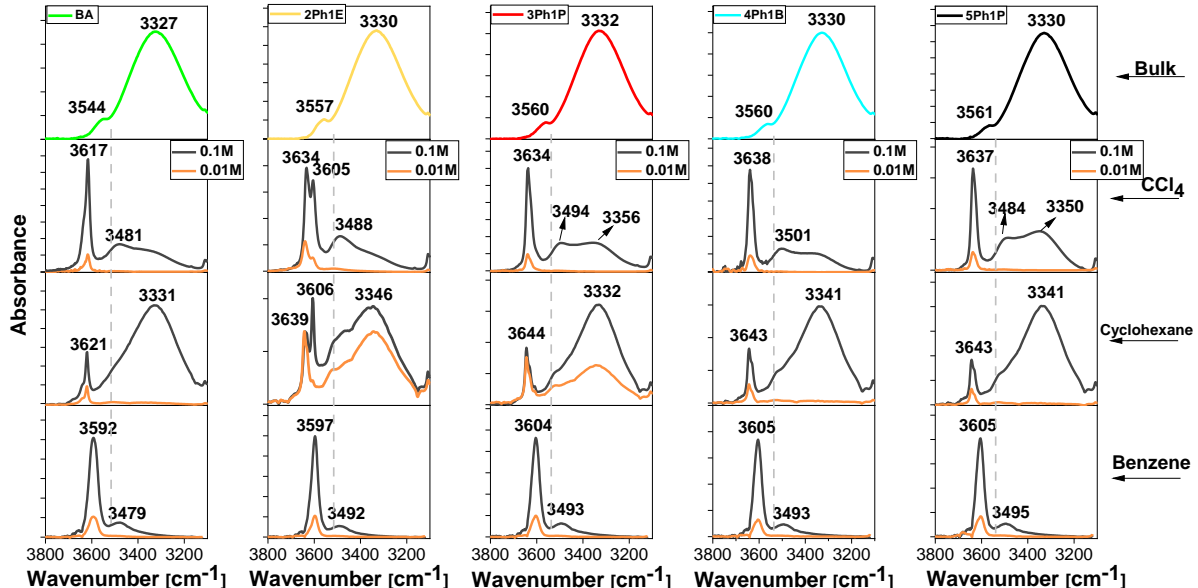


**Figure S3.** FTIR spectra of PhAs in bulk and dissolved in non-polar solvents (CCl<sub>4</sub>, cyclohexane, benzene) in the range of 3800 – 3100 cm<sup>-1</sup>.

**Table S1.** The peak wavenumber, integral intensity, full-width at half maximum (*FWHM*), and the estimated values of free OH bonds as well as the degree of OH association for analyzed PhAs.

Material	Peak wavenumber [cm <sup>-1</sup> ]					
	<i>T</i> = 368 K		<i>T</i> = 293 K		<i>T<sub>g</sub></i>	
	OH <sub>bonded</sub>	OH <sub>free</sub>	OH <sub>bonded</sub>	OH <sub>free</sub>	OH <sub>bonded</sub>	OH <sub>free</sub>
PhM	3381	3560	3322	3544		
2Ph1E	3404	3568	3329	3557	3278	--
3Ph1P	3386	3573	3332	3559	3282	--
4Ph1B	3396	3568	3330	3560	3278	--
5Ph1P	3396	3587	3329	3568	3282	--
7Ph1H	3394	3585	3331	3567		--
Integral intensity [a.u.]						
PhM	188,68	8,48	259,65	5,58	--	--
2Ph1E	184,80	10,72	256,33	6,76	457,14	--
3Ph1P	190,54	8,50	278,81	5,32	380,21	--
4Ph1B	102,67	4,46	174,74	3,02	233,02	--
5Ph1P	110,22	4,37	182,49	2,71	247,51	--
7Ph1H	104,40	3,76	184,05	2,53	--	--
Total integral intensity [a.u.]						
PhM	197,16		265,23			
2Ph1E	195,52		263,09		457,14	
3Ph1P	199,04		284,13		380,21	
4Ph1B	107,13		177,76		233,02	
5Ph1P	114,59		185,20		247,51	
7Ph1H	108,16		186,58			
FWHM [cm <sup>-1</sup> ]						
PhM	295.07		250.07		--	--
2Ph1E	287.85		240.01		193.76	--
3Ph1P	273.44		236.31		203.11	--
4Ph1B	285.61		237.98		207.68	--
5Ph1P	278.98		238.12		206.74	--
7Ph1H	278.59		242.04		--	
Content of free OH groups [%]						
PhM	4,3		2,1		--	
2Ph1E	5,4		2,6		--	

3Ph1P	4,2	1,8	--
4Ph1B	4,1	1,7	--
5Ph1P	3,8	1,4	--
7Ph1H	3,4	1,3	--
<b>Degree of associated OH groups [%]</b>			
PhM	95,7	97,7	—
2Ph1E	94,6	97,4	--
3Ph1P	95,8	98,2	--
4Ph1B	95,9	98,3	—
5Ph1P	96,2	98,6	—
7Ph1H	96,6	98,7	—

The anti-symmetric and symmetric stretching of the aliphatic CH groups ( $\nu_{CH,alkyl}$ ) are detected between 3000 and 2750  $\text{cm}^{-1}$ , while the ones originating from the aromatic CH groups can be seen at 3150 and 3000  $\text{cm}^{-1}$  ( $\nu_{CH,ring}$ ). It is observed that a higher number of  $\text{CH}_2$  groups in the alkyl chain results in a stronger (more intense) symmetric and anti-symmetric  $\text{CH}_2$  vibration signal. As shown in **Figure S4**, a change in the position of alkyl CH bands with the elongation of the hydrocarbon chain was detected, i.e., the higher the number of  $\text{CH}_2$  units in the hydrocarbon chain, the lower the wavenumber value of the symmetric CH stretching vibrations. The opposite trend was only seen for the  $\nu_{CH,alkyl}$  band of PhM occurring at 2930  $\text{cm}^{-1}$ , where adding of  $\text{CH}_2$  unit to hydrocarbon chain results in the increase of frequency (to 2943  $\text{cm}^{-1}$  for 2Ph1H). However, the further increasing number of  $\text{CH}_2$  groups (from 2Ph1H to 7Ph1H) causes the red-shift of this band. On the other hand, the  $\nu_{CH,ring}$  band positions exhibit a slight dependence on the alkyl chain length, i.e., a very weak red-shift was observed for 3030, 3064, and 3088  $\text{cm}^{-1}$  lines when going from PhM to 3Ph1H (**Figure S5**). Then, the position of the  $\nu_{CH,ring}$  signals remained constant, although there was a change in the number of methylene groups (from 3Ph1H to 7Ph1H).

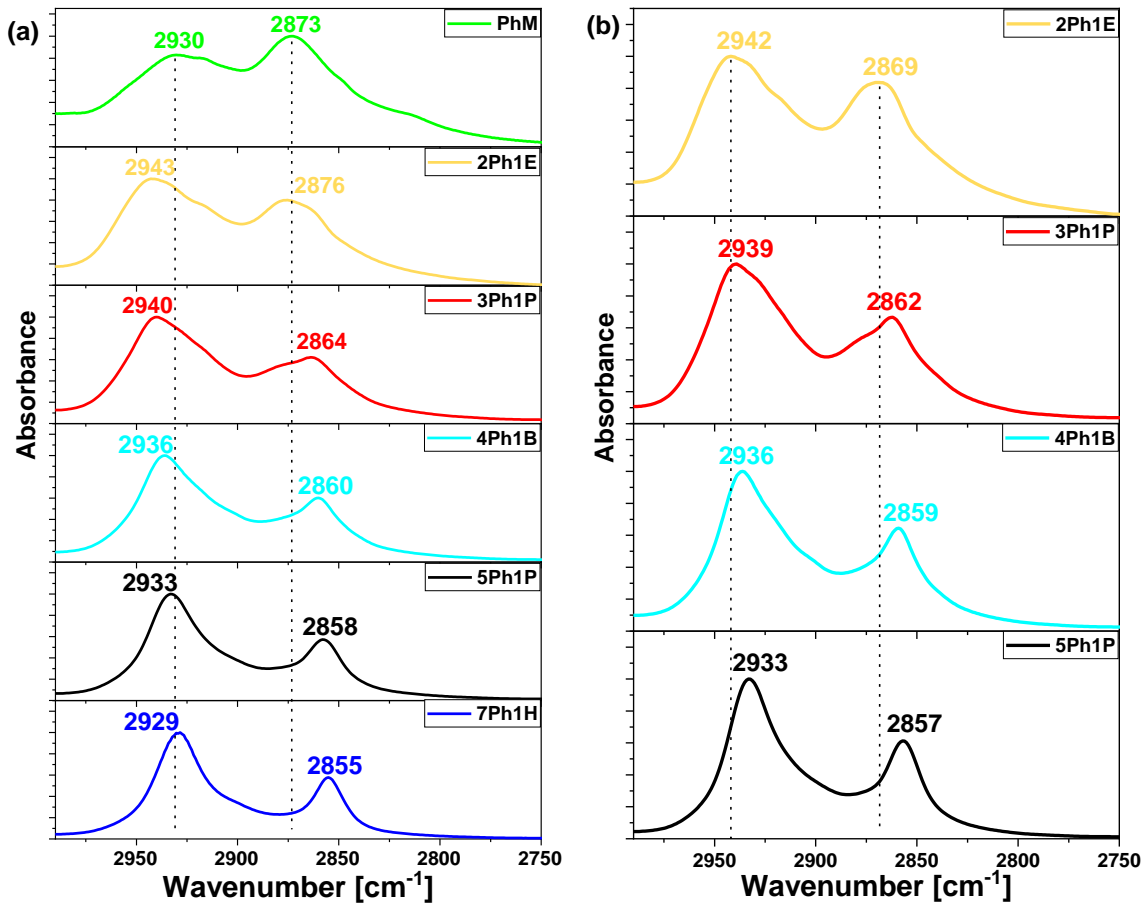


**Figure S4.** FTIR spectra of the stretching vibration bands of the CH aliphatic groups of PhAs in the temperature (a) 293 K and (b)  $T_g$ . The spectra were normalized to the maximum intensity of the CH band.

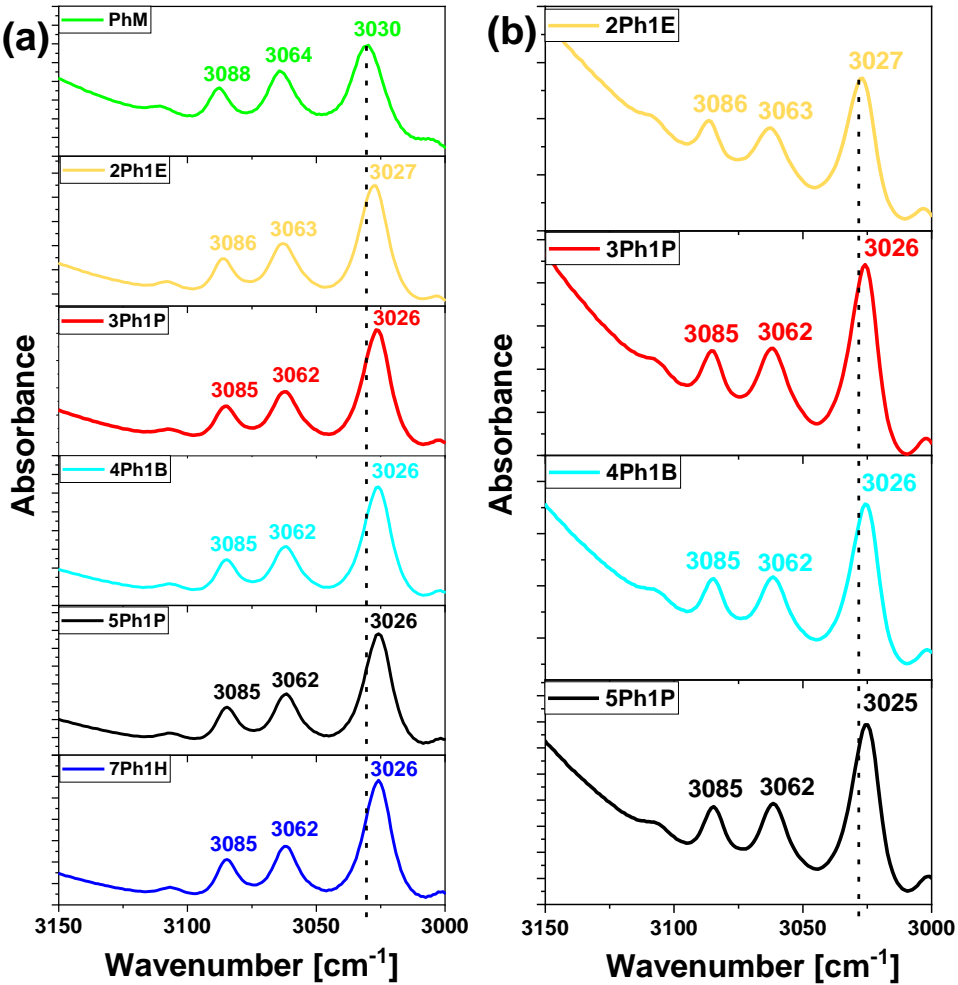


**Figure S5.** FTIR spectra of the stretching vibration bands of the CH ring groups of PhAs in the temperature (a) 293 K and (b)  $T_g$ .

As demonstrated in **Figures S6a,b**, PhM and 7Ph1H show nearly the same  $\nu_{OH}$  band shape at 293 K, suggesting a similar way of the self-assembling process at this temperature. In contrast, at 223 K, a significant difference between the shape of their spectra can be seen, i.e., PhM exhibits a single broad  $\nu_{OH,assoc}$  band similar to that in the liquid phase, whereas for the crystalline 7Ph1H, two distinguishable components of the  $\nu_{OH,assoc}$  band appear, which do not resemble that registered for the liquid. It means that in the liquid and crystalline states, PhM forms similar supramolecular clusters, through strong O–H···O hydrogen bonds and a surrogate C–H··· $\pi$  interactions,<sup>1</sup> whereas in 7Ph1H different HB clusters are formed, in terms of the geometry and/or size. Thus, these findings very well correlate with the XRD results described above. The doublet structure of the  $\nu_{OH,assoc}$  band of crystalline 7Ph1H can be explained by two alternative mechanisms, namely: *i*) two different types of O–H···O hydrogen bonds with alternating O···O distances are formed in the polar region of this PhA, or *ii*) the coupling phenomena gives rise to two subbands originating from the in-phase and out-of-phase coupled vibrations of adjacent O–H bonds along with the O–H···O H-bond network.<sup>2</sup>

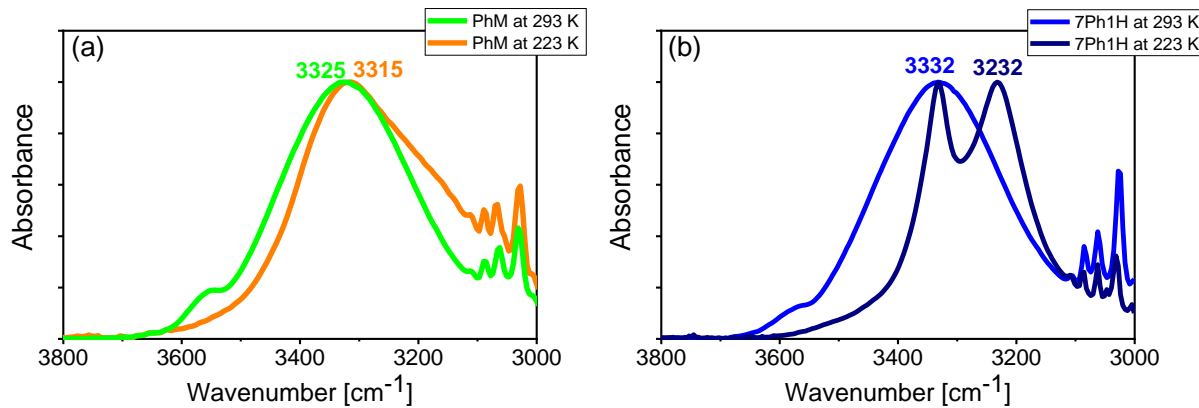


**Figure S6.** FTIR spectra of (a) PhM liquid at 293 K and crystal at 223 K; (b) 7Ph1H liquid at 293 K and crystal at 223 K. The spectra were normalized to the OH stretching vibration intensity peak.

#### Determination of the activation enthalpy for the dissociation process from FTIR spectroscopy measurements

The activation enthalpy for the dissociation process was calculated using the van't Hoff equation, which relates the change in the equilibrium constant,  $K$ , of dissociation to the change in temperature,  $T$ , according to the relation:

$$\ln K = -\frac{E_a}{RT} + \frac{\Delta S}{R}, \quad (1)$$

where  $E_a$  is activation enthalpy, and  $\Delta S$  is the entropy of the dissociation process. For this purpose, the FTIR spectra of the studied alcohols were measured as a function of temperature in the range 298 - 373 K. To obtain the plots of  $\ln K$  versus  $1/T$ , the deconvolution of the  $\nu_{OH}$  bands was performed. The procedure of determination of the integral intensity,  $A$ , values of  $\nu_{OH,assoc}$  and  $\nu_{OH,free}$  bands was described in more detail in our previous work.<sup>3</sup> In **Figure S7**, the van't Hoff plots were presented.

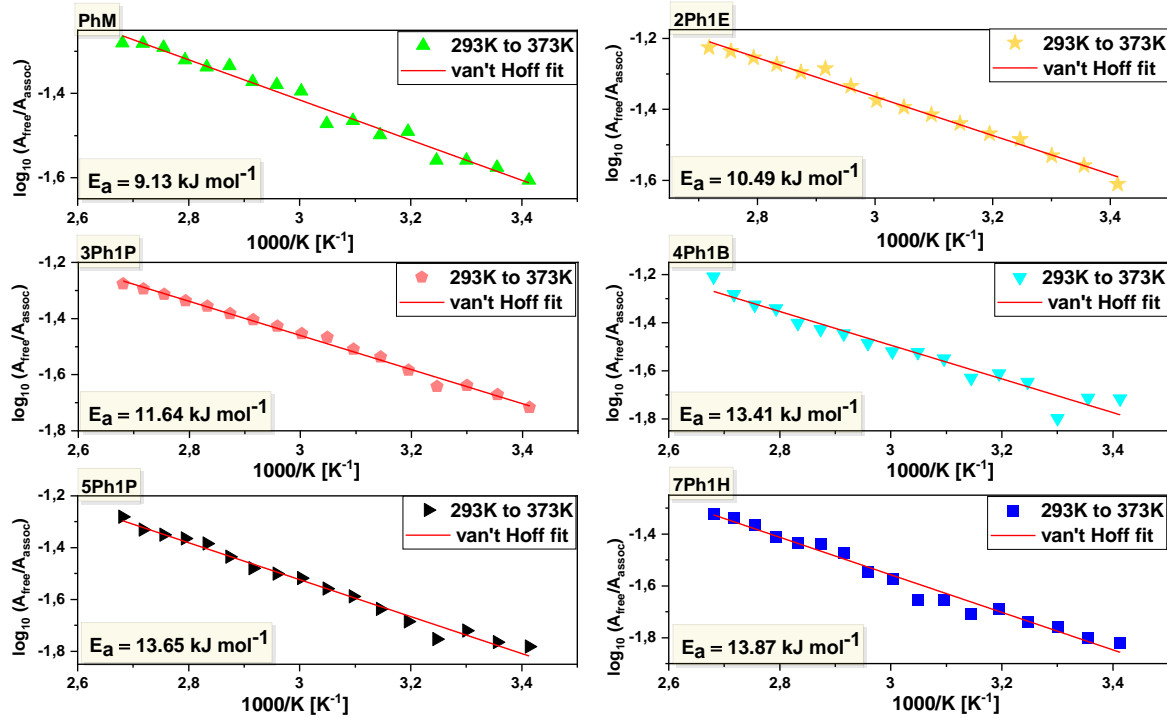


**Figure S7.** The van't Hoff plots for the IR absorption bands of (a) PhM, (b) 2Ph1E, (c) 3Ph1P, (d) 4Ph1B, (e) 5Ph1P and (f) 7Ph1H used to extract the dissociation enthalpy between the H-bonded and free OH species.

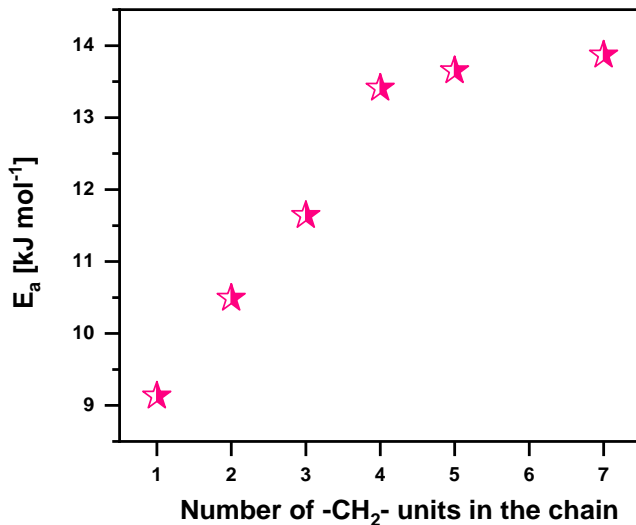


**Figure S8.** Activation energy dependency of the number of  $-\text{CH}_2-$  units in the aliphatic chain of the studied PhAs.

**Table S2.** The values of the activation enthalpy of dissociation process,  $E_a$ , and the average number of H-bonded molecules in the supramolecular assemblies,  $n$ , for measured PhAs.

Material	$E_a$ [kJ mol <sup>-1</sup> ]	$n$ value
PhM	$9.13 \pm 0.34$	2.89
2Ph1E	$10.49 \pm 0.28$	2.44
3Ph1P	$11.64 \pm 0.25$	2.85
4Ph1B	$13.41 \pm 0.80$	2.87 [ <sup>4</sup> ]
5Ph1P	$13.65 \pm 0.43$	2.9
7Ph1H	$13.87 \pm 0.57$	--

### Results of the solution state FTIR spectroscopy

The investigation of the average number of H-bonded PhA molecules in the cluster was performed using the procedures described in our previous works.<sup>4</sup> The  $n$  value is found to be between 2 (2Ph1E) and 3 (other PhAs) (**Figure S9; Table S2**). The  $n$  value for 4Ph1B, determined in our previous work<sup>4</sup>, is equal to 2.9 (**Table S2**). These data imply that PhAs form, on average, the H-bonded dimers or trimers, which agrees with the results obtained by <sup>1</sup>H NMR method.<sup>5</sup> It is worth noting that the degree of association by HBs in dissolved PhAs appears to be independent of the extent of van der Waals or hydrophobic interactions in these solutions. A similar effect was detected in literature for alcohols dissolved in carbon tetrachloride solutions with a number of carbon atoms in the skeleton from 1 to 18.<sup>6</sup>

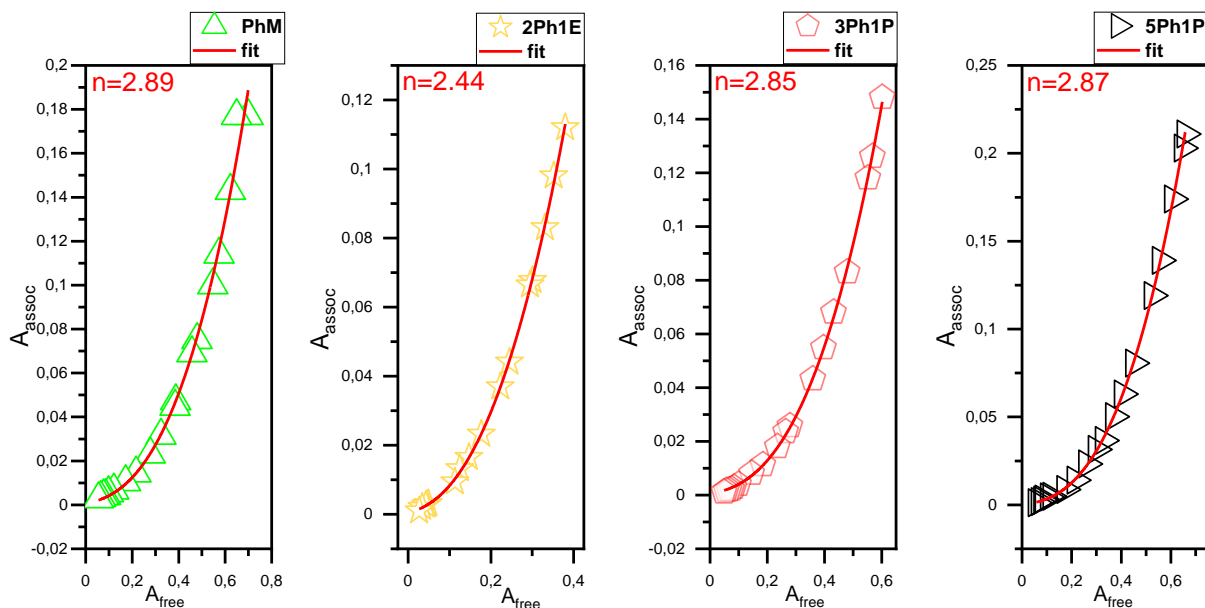


**Figure S9.**  $A_{assoc}$  versus  $A_{free}$  dependencies, red lines are the best fits for Equation 2. The intercept of the line on the ordinate axis at zero gives the value of the degree of association ( $n$ ).

## Results of Density Functional Theory (DFT) computations

The O atom of the hydroxyl group has a more negative charge than other atoms (the largest electronic density) because of the electronegativity property (**Figure S10, Table S3**). In contrast, the H atom belonging to the OH group and the C atom bonded to the OH group have a positive charge, indicating possible sites/regions for nucleophilic attack. The charges of the C atoms of the phenyl ring are found to be either positive (the C<sub>4</sub>) or negative (the C<sub>1</sub>, C<sub>2</sub>, and C<sub>3</sub> atoms). Thus, the obtained charges may give information about the regions where the compound can have intermolecular interactions. What is more, the Mulliken and CHelpG charge values depend on the number of the CH<sub>2</sub> groups in the side alkyl chain and vary as the electronic density re-distributes within the molecule. As can be seen, CHelpG charges of the C<sub>4</sub> and C<sub>OH</sub> atoms demonstrate especially great variability going from PhM to 3Ph1P, and then these values are rather slightly alkyl chain dependent. Interestingly, the C<sub>4</sub> atom for 2Ph1E shows the most negative value, probably suggesting the formation of a weak intermolecular C<sub>4</sub>-H···O HBs (the charge transfer from the O atom acting as the acceptor towards the HB donor), which may additionally stabilize the supramolecular network of 2Ph1E. An odd-even alternation of CHelpG atomic charges is slightly observed with the elongation of the analyzed PhAs that additionally confirms the variation of experimental data.

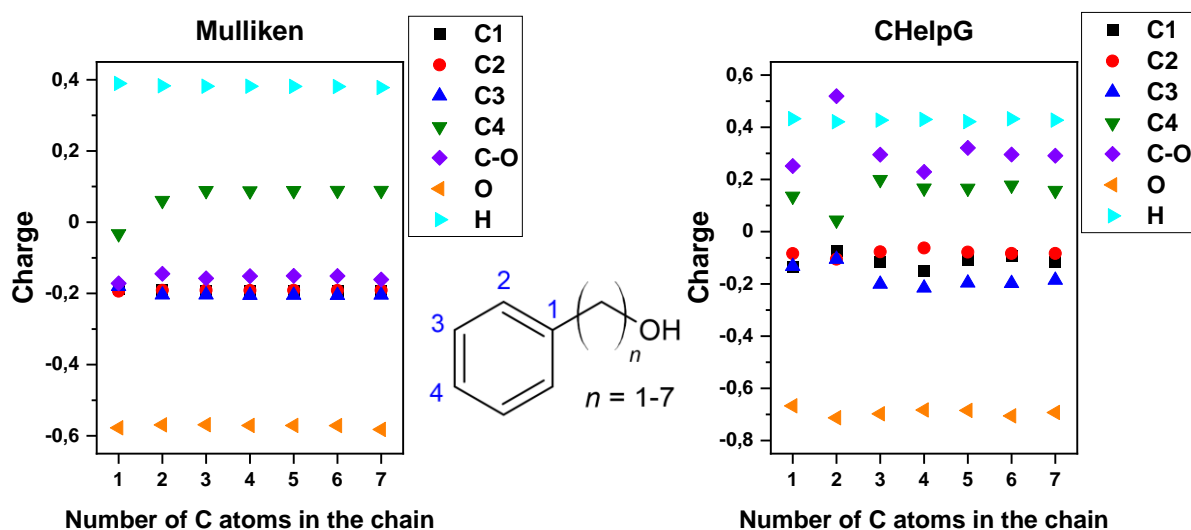


**Figure S10.** The variation in charge with increasing alkyl chain for PhAs using Mulliken (left) and CHelpG (right) methods. As insert a chemical structure of PhAs with numbered carbon atoms in the benzene ring.

**Table S3.** Atomic partial charges calculated in the framework of the density functional theory.

Number of C atoms in the alkyl chain	C1	C2	C3	C4	C-O	O	H
<b>Mulliken</b>							
0	-0.194072	-0.190969	-0.210616	0.205684		-0.584853	0.396589
1	-0.18863	-0.19374	-0.180213	-0.03277	-0.17198	-0.577661	0.389391
2	-0.191399	-0.191184	-0.20422	0.0607	-0.145076	-0.569087	0.382898
3	-0.1916	-0.191236	-0.204196	0.088554	-0.157939	-0.568757	0.381666
4	-0.192033	-0.191532	-0.205494	0.087802	-0.151565	-0.570988	0.381533
5	-0.191886	-0.191399	-0.205131	0.088582	-0.150661	-0.570922	0.381112
6	-0.192114	-0.191567	-0.205509	0.088822	-0.150981	-0.571357	0.381036
7	-0.192102	-0.191393	-0.204714	0.088955	-0.161006	-0.581989	0.37788
<b>CHelpG</b>							
0	-0.159222	-0.053297	-0.235413	0.39123		-0.560576	0.365171
1	-0.134983	-0.083954	-0.132311	0.135713	0.251518	-0.667158	0.432624
2	-0.075265	-0.105277	-0.105277	0.044029	0.519029	-0.712708	0.421042
3	-0.116534	-0.077079	-0.200997	0.199474	0.295165	-0.69764	0.427203
4	-0.151565	-0.062404	-0.215583	0.166796	0.229117	-0.683053	0.429812
5	-0.108496	-0.078046	-0.196233	0.16619	0.320991	-0.684484	0.421508
6	-0.094185	-0.083397	-0.198021	0.178192	0.295562	-0.705649	0.432167
7	-0.116603	-0.08354	-0.185801	0.157923	0.290935	-0.692426	0.427252

## Results of Surface tension measurements

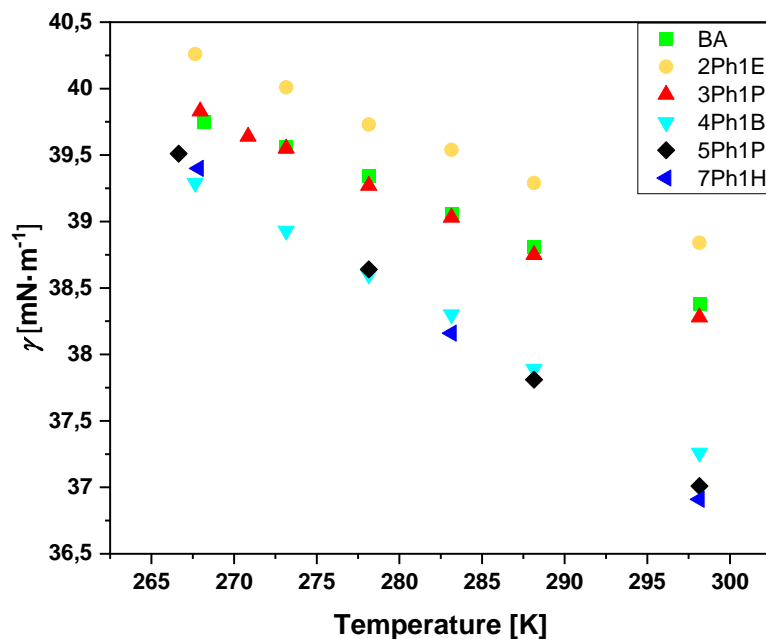


**Figure S11.** Surface tension of PhAs at different temperatures.

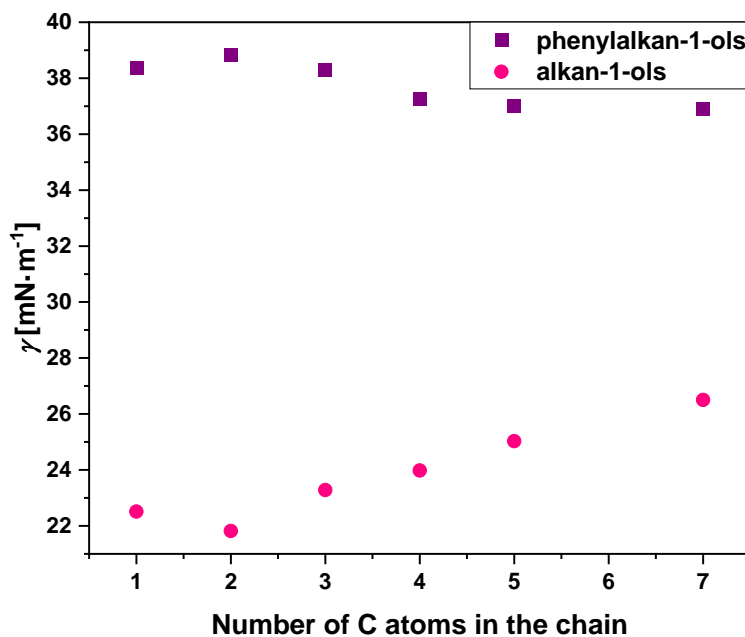


**Figure S12.** Surface tension of PhAs and alkyl alcohols (data from Ref. 7 and 8) for comparison.

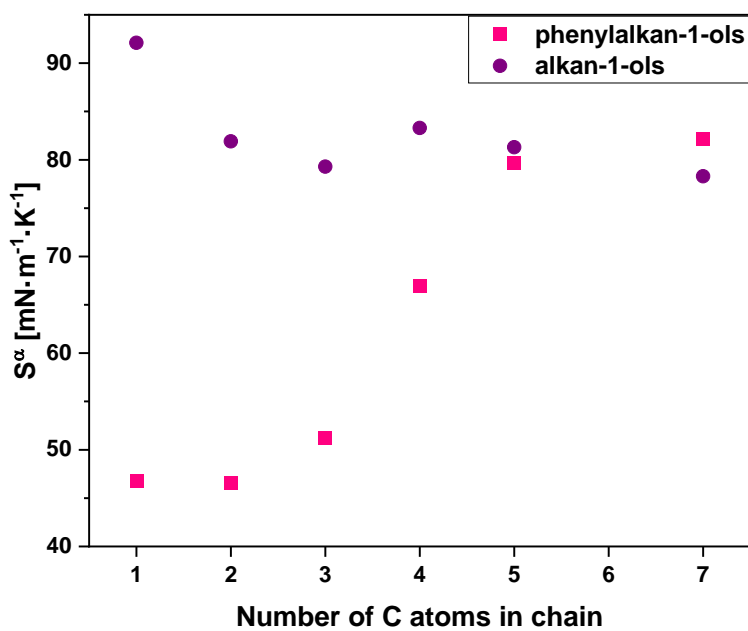


**Figure S13.** Surface entropy ( $S^a = -\left(\frac{\partial \gamma}{\delta T}\right)_p$ , mN·m<sup>-1</sup>·K<sup>-1</sup>) of PhAs and alkyl alcohols (calculated based on literature data Ref. 7 and 8) for comparison.

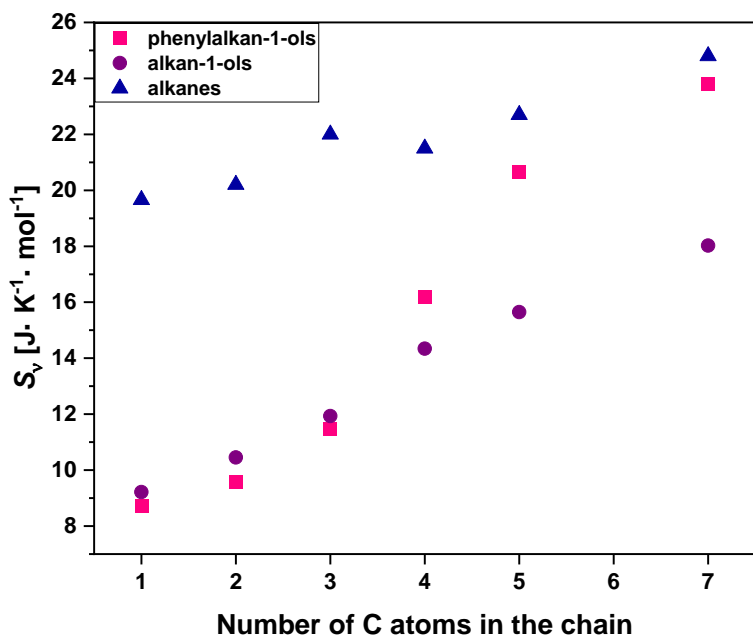


**Figure S14.** Molar surface entropy ( $S_v = -8.45 \cdot V_m^{2/3} \cdot \left(-\frac{\partial \gamma}{\delta T}\right)_p$ , J·K<sup>-1</sup>·mol<sup>-1</sup>) of PhAs, alkyl alcohols (calculated based on literature data Ref. 7 and 8), and alkanes (taken from Ref. 9) for comparison.

**Table S4.** Surface tension ( $\gamma$ ), surface entropy ( $S^a$ ), and molar surface entropy ( $S_v$ ) estimated at  $T = 298$  K for the investigated systems.

Material	Surface Tension, $\gamma$ [mN·m <sup>-1</sup> ]	Surface entropy, $S^a$ $10^3 \cdot [\text{mN} \cdot \text{m}^{-1} \cdot \text{K}^{-1}]$	Molar surface entropy, $S_v$ [J·K <sup>-1</sup> mol <sup>-1</sup> ]
BA	38.38	46.8	8.74
2Ph1E	38.84	46.6	9.59
3Ph1P	38.28	51.2	11.47
4Ph1B	37.26	67.0	16.21
5Ph1P	37.01	79.7	20.65
7Ph1H	36.91	82.2	23.81

<sup>1</sup> S. K. Nayak, R. Sathishkumar and T. G. Row, *CrystEngComm*, 2010, **12**(10), 3112-3118.

<sup>2</sup> V. Andrushchenko and W. Pohle, *Phys. Chem. Chem. Phys.*, 2019, **21**, 11242–11258.

<sup>3</sup> N. Soszka, B. Hachuła, M. Tarnacka, E. Kaminska, S. Pawlus, K. Kaminski and M. Paluch, *J. Phys. Chem. B.*, 2021, **125**(11), 2960-2967.

<sup>4</sup> K. Jurkiewicz, S. Kołodziej, B. Hachuła, K. Grzybowska, M. Musiał, J. Grelska, R. Bielas, A. Talik, S. Pawlus, K. Kamiński and M. Paluch, *J. Mol. Liq.*, 2020, **319**, 114084.

<sup>5</sup> T. Schaefer, R. Sebastian, J. Peeling, G. H. Penner and K. Koh, *Can. J. Chem.*, 1989, **67**, 1015.

<sup>6</sup> L. Wilson, R. Bicca de Alencastro and C. Sandorfy, *Can. J. Chem.*, 1985, **63**, 4045.

<sup>7</sup> G. Vázquez, E. Alvarez and J. M. Navaza, *J. Chem. Eng. Data*, 1995, **40**, 611-614.

<sup>8</sup> Yu. V. Efremov, *Zh. Fiz. Khim.*, 1966, **40**, 1240–1247.

<sup>9</sup> R. T. Myers, *J. Colloid Interface Sci.*, 2004, **274**, 229–236.